Int J Adv Manuf Technol (2009) 43:264–275
DOI 10.1007/s00170-008-1705-0

ORIGINAL ARTICLE

Investigation of machining parameters for the multiple-response optimization of micro electrodischarge milling

Reyad Mehfuz · Mohammad Yeakub Ali

Received: 29 April 2008 / Accepted: 11 August 2008 / Published online: 28 August 2008

Abstract This paper investigated the influence of three micro electrodischarge milling process parameters, which were feed rate, capacitance, and voltage. The response variables were average surface roughness (R_a), maximum peak-to-valley roughness height (R_y), tool wear ratio (*TWR*), and material removal rate (*MRR*). Statistical models of these output responses were developed using three-level full factorial design of experiment. The developed models were used for multiple-response optimization by desirability function approach to obtain minimum R_a, R_y, *TWR*, and maximum *MRR*. Maximum desirability was found to be 88%. The optimized values of R_a, R_y, *TWR*, and *MRR* were 0.04, 0.34 μm, 0.044, and 0.08 mg min^{-1}, respectively for 4.79 μm s^{-1} feed rate, 0.1 nF capacitance, and 80 V voltage. Optimized machining parameters were used in verification experiments, where the responses were found very close to the predicted values.

Keywords Micro ED milling · Multiple-response optimization · Surface roughness · Tool wear ratio · Material removal rate

1 Introduction

Miniaturization of components is perceived as a requirement for the future technological development in electronics, biomedical engineering, aerospace, military applications, etc. Applications of microsystems to enhance health care, quality of life, and economic growth grabbed huge attention of the commercial industries. Some examples are microchannels for micro fuel cell, lab-on-chips, shape memory alloy "stents," fluidic graphite channels for fuel cell applications, miniature actuators and sensors, medical devices, etc. [1, 2]. The current research trend is to develop simpler and cheaper processes to fabricate miniaturized products. The common techniques for product miniaturization are based on silicon processing techniques, where silicon-based materials are processed through wet and dry chemical etching. These techniques are suitable for microelectronics, limited to a few silicon-based materials and restricted to simple two-dimensional (2D) or pseudo three-dimensional (2.5D) planar geometries. Other fabrication processes, such as LiGA (lithography, electroforming, and molding), laser, ultrasonic, focused ion beam, micro electrodischarge machining (EDM), mechanical micromilling, etc. are expensive and require high capital investment. Moreover, these processes are limited to selected materials and low throughput [3]. Among the tool-based micromachining processes, micro electrodischarge (ED) milling has great prospects in the fabrication of micro features. Its specialty includes the ability of fabricating micro features of wide varieties of materials with complex 3D geometries, which are not possible by lithography or etching processes. Micro ED milling is an effective way to fabricate complex contour micromold and hot embossing master microtool. This micromold or master microtool can be used for mass replication. The motivation of using micro ED milling comes from the translation of the knowledge obtained from the conventional EDM process to the microlevel. However, the principle of die-sinking micro EDM is not directly applicable to micro ED milling. In die-sinking micro EDM, the occurrence of the high tool wear necessitates the use of multiple tools with increasing dimensions to produce the

R. Mehfuz (✉) · M. Y. Ali
Department of Manufacturing and Materials Engineering,
Faculty of Engineering, International Islamic University Malaysia,
P.O. Box 10, 50728 Kuala Lumpur, Malaysia
e-mail: rmehfuz@yahoo.com

desired geometry and accuracy [4]. The design and fabrication of multiple microscale tools are very time-consuming and costly. Moreover, complex contour shapes cannot be produced by die-sinking micro EDM. Therefore, micro ED milling is becoming a more economic alternative to die-sinking micro EDM [5].

In micro ED milling, the material is eroded by noncontact thermoelectrical process, which is similar to micro EDM. A series of discrete sparks occur between the workpiece and the rotating tool electrode. The workpiece and tool are immersed in a dielectric fluid. The dielectric fluid is continuously fed to the machining zone to convey the spark and flush away the eroded particles. The work feeding system of micro ED milling is similar to mechanical end milling process. The workpiece is fed to the tool electrode while the tool is in rotation. The movement of tool is controlled numerically to achieve the desired shape and accuracy of the workpiece. Figure 1 shows the schematic of the micro ED milling process.

Micro ED milling has a number of process parameters, which are influential on the machining performance. Depending upon the circuit type used in the machine, the importance of parameters is also varied. Some researches were conducted to optimize different EDM process parameters for R_a, R_y, *TWR*, and *MRR* [6, 7]. But almost all of them were on conventional macro EDM. The full understanding of micro ED milling process parameters are yet to be developed, as the process itself is a new branch of manufacturing.

The roughness of machined surface is influenced by discharge energy. It was experimentally investigated that with the increase in discharge energy either by increasing voltage or capacitance, R_a increased in die-sinking EDM, wire EDM, and wire electrodischarge grinding [8–10]. A large discharging energy usually causes violent sparks and results in a deeper erosion crater on the surface. Accompanying the cooling process after the spilling of molten metal, residues remain at the periphery of the crater to form a rough surface [11]. Thermal models were developed for R_a and R_y or R_{max} for die-sinking micro EDM [12]. It showed that, with the increase in current and pulse duration, surface roughness increased. EDM-generated surface roughness of ceramic was also investigated. EDM of boron carbide (B_4C) showed that R_a and R_y increased with pulse duration but decreased with current [6]. On the other hand, EDM of high-speed steel showed that with current R_a increased while with pulse duration it decreased [7]. It was suggested to use low conductive or higher resistive dielectric to ensure low R_a and R_y [11]. Use of rotating electrode was helpful for high shape accuracy and higher *MRR* but it caused higher surface roughness [13]. There was no analysis reported on the effect of feed rate on machined surface.

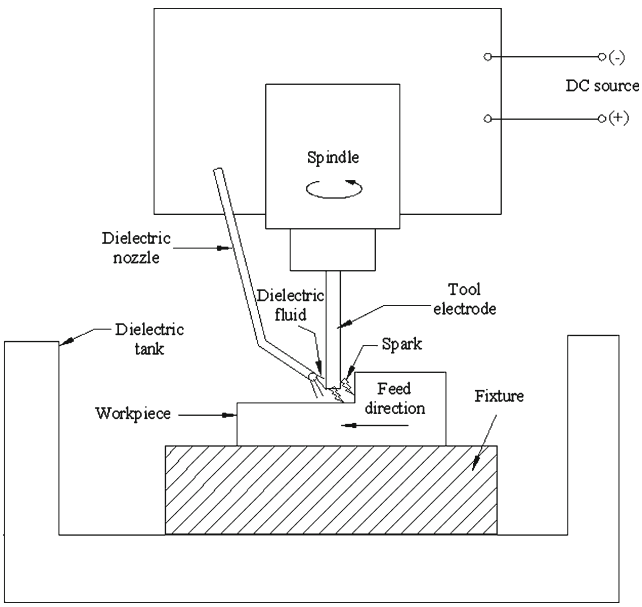

Fig. 1 Schematic of micro ED milling

The wear of tool electrode is responsible for shape inaccuracy and dimensional instability. At higher feed rate, tool wear was found decreasing [4]. It was also observed that tool wear was increasing with feed rate but after reaching the peak it started decreasing [14]. High discharge energy usually caused high *TWR* [8]. In EDM of high-speed steel and boron carbide (B_4C), tool wear was found rising with current and falling with pulse duration [6, 7]. It was also found that tool wear showed an optimum peak value while pulse duration had increased [15]. However, use of shorter pulse on time was suggested to achieve lower *TWR* [16].

The negative polarity of the tool gives a lower tool wear than that of positive polarity in the range of low to medium discharge current values. At high current settings, the polarity has no significant effect on tool wear. A slight decrease in *TWR* was observed with increasing current in negative polarity. In the case of positive polarity, *TWR* decreased significantly with increasing current [17].

The type of dielectric fluid is also responsible for tool wear rate. Kerosene is frequently used as the dielectric medium. In EDM, carbide layer formed on the workpiece surface with the use of kerosene, which has a higher melting temperature than the oxide layer formed with the use of distilled water. The carbide layer formed by kerosene needed higher pulse energy for melting and evaporation which caused high tool wear [18]. The use of low resistive deionized water as a dielectric fluid resulted in reduced tool wear compared to kerosene [19].

Experimental investigation in conventional EDM found that *MRR* increased with the discharge current. With the increase in pulse duration, *MRR* showed a peak and then downfall [7, 12]. Increase in discharge energy by discharge voltage or capacitance resulted in higher *MRR* [14]. Lower material removal depth was observed with the increase in

feed rate [4]. *MRR* can be increased in both positive and negative polarity by rotating the tool electrode [13]. Higher *MRR* was obtained for low ultrasonic vibration frequency combined with tool rotation [20].

Dielectric flushing system is also responsible for the variation in *MRR*. The low *MRR* in static condition is mainly due to improper flushing of the molten and evaporated workpiece material from the machining gap [15]. With the increase in flushing flow rate, *MRR* increased. Use of kerosene and tap water as the dielectric fluid showed higher *MRR* than distilled water [18].

This paper focuses on the use of micro ED milling to achieve minimum R_a and R_y with higher *MRR* and lower *TWR*. It examines and explains the influence of three process parameters, e.g., feed rate, capacitance, and voltage, on the output responses. Statistical models have been developed using three-level full factorial experimental design. The paper explains the use of developed models for multiple-response optimization. Experimental verification of the models was also discussed.

2 Experiments

In this subsection, the experimental design used to conduct the experiments are briefly discussed. Selection of workpiece, tool materials, and the equipments used are also addressed.

2.1 Experimental design

The experiment was designed based on three-level full factorial statistical model, which was chosen to observe and analyze the individual influences as well as the interaction effects of the three process parameters on R_a, R_y, *TWR*, and *MRR*. A total number of 32 experiments was conducted, which includes five repeated experiments at the same middle values of the parameters. The experimental conditions are shown in Table 1.

The definition of response parameters are as follows:

$$R_a = \text{Average surface roughness}$$
$$R_y = \text{Maximum peak} - \text{to} - \text{valley roughness height}$$
$$TWR = \frac{\text{Volume of tool wear}}{\text{Volume of workpiece wear}}$$
$$MRR = \text{Weight of material removed perunit time}$$

2.2 Workpiece and tool materials

Beryllium–copper (Be–Cu) alloy (Be=0.4%, Ni=1.8%, Cu=97.8%), which is also known as Protherm, was selected as the workpiece material. It possesses very high thermal conductivity (245 Wm^{-1} $°C^{-1}$), high temperature resistance, and high corrosion resistance. These features enable it to become a suitable mold material. As the tool electrode material, tungsten (W) was chosen because of its low wear rate. The electrode diameter was 0.5 mm.

2.3 Equipment and procedures

A commercial multipurpose micro machine tool (DT 110, Mikrotools, Singapore) containing micro EDM facilities with a resistance capacitance (RC) circuit was used to perform the experiments. RC circuit ensures low discharge current with higher frequency and thus, suitable in microscale electric discharge. As the dielectric liquid, EDM-3 synthetic oil was used for the experiments. The tool

Table 1 Experimental conditions

		Experimental conditions		
		Level		
	Factors	1	2	3
Controlled parameters				
Feed rate (μm/s)	A	2.00	4.00	6.00
Capacitance (nF)	B	0.10	1.00	10.00
Voltage (V)	C	80	100	120
Fixed parameters				
Tool electrode		Tungsten		
Workpiece		Be–Cu alloy		
Tool electrode diameter (mm)		0.50		
Spindle speed (rpm)		2,000		
Polarity		Workpiece+ve		
Dielectric fluid		EDM-3 (synthetic oil)		
Machining length (mm)		13.00		
Machining depth (mm)		0.20		

electrode was clamped in the spindle, while the workpiece was fixed in the worktable. After clamping, the spindle was rotated at a speed of 2,000 rev min^{-1} while the worktable was fed. Figure 1 schematically depicts the experimental setup. To determine the *MRR* and *TWR*, workpieces and tool electrodes were weighed before and after each experiment, using an electric balance (B204-S Mettler Toledo, Switzerland) with a resolution of 100 μg,. The surface roughness was measured by using a precision surface profiler (Mitutoyo, Surftest SV-500). After ultrasonic cleaning, the machine work surface was inspected by scanning electron microscope (SEM; JEOL JSM-5600).

3 Results and discussions

The experimental results of all the responses, R_a, R_y, *TWR*, and *MRR*, are tabulated in Table 2. Analysis of variance (ANOVA) approach was used to check the adequacy of the model. The analysis ultimately showed the main and interaction effects of the process variables on the responses. Main effect was the direct effect of an independent variable while interaction effect was the joint effect of two independent variables on the responses.

3.1 Calculation of ANOVA

ANOVA results for R_a, R_y, *TWR*, and *MRR* are shown in the Tables 3, 4, 5, and 6, respectively. These tables show the statistical significance of each effect by means of the comparison of the mean squares (MS) with an estimation of the experimental error. In the table, SS represents sum of squares while *df* represents the number of degrees of freedom. The column corresponding to MS is obtained simply by dividing SS by its corresponding *df*. In contrast, the column of *F* value is calculated as the quotient of each of the MS of the effects divided by the value of the MS corresponding to the residual. Column of probability values

Table 2 Design matrix of the experiment and measured responses

Exp no.	Feed rate (μm s^{-1})	Capacitance (nF)	Voltage (V)	R_a (μm)	R_y (μm)	*TWR*	*MRR* (mg min^{-1})
1	2.00	0.10	80.00	0.04	0.31	0.121	0.02
2	4.00	0.10	80.00	0.04	0.35	0.044	0.07
3	6.00	0.10	80.00	0.04	0.36	0.133	0.09
4	2.00	1.00	80.00	0.10	0.78	0.154	0.04
5	4.00	1.00	80.00	0.12	0.91	0.066	0.09
6	6.00	1.00	80.00	0.10	0.89	0.165	0.09
7	2.00	10.00	80.00	0.44	3.23	0.182	0.06
8	4.00	10.00	80.00	0.44	3.21	0.089	0.10
9	6.00	10.00	80.00	0.48	3.53	0.220	0.11
10	2.00	0.10	100.00	0.05	0.49	0.165	0.03
11	4.00	0.10	100.00	0.05	0.40	0.049	0.09
12	6.00	0.10	100.00	0.06	0.54	0.157	0.09
13	2.00	1.00	100.00	0.19	1.28	0.194	0.06
14	4.00	1.00	100.00	0.17	1.20	0.065	0.16
15	6.00	1.00	100.00	0.18	1.38	0.186	0.14
16	2.00	10.00	100.00	0.53	3.99	0.239	0.10
17	4.00	10.00	100.00	0.54	4.08	0.098	0.35
18	6.00	10.00	100.00	0.53	4.05	0.216	0.13
19	2.00	0.10	120.00	0.05	0.44	0.198	0.06
20	4.00	0.10	120.00	0.07	0.52	0.065	0.15
21	6.00	0.10	120.00	0.08	1.23	0.166	0.10
22	2.00	1.00	120.00	0.19	1.81	0.227	0.07
23	4.00	1.00	120.00	0.17	1.22	0.086	0.36
24	6.00	1.00	120.00	0.18	1.37	0.198	0.14
25	2.00	10.00	120.00	0.56	3.11	0.261	0.16
26	4.00	10.00	120.00	0.62	3.79	0.128	0.41
27	6.00	10.00	120.00	0.54	3.77	0.247	0.15
28	4.00	1.00	100.00	0.22	1.30	0.058	0.10
29	4.00	1.00	100.00	0.22	1.53	0.072	0.49
30	4.00	1.00	100.00	0.15	1.06	0.067	0.24
31	4.00	1.00	100.00	0.19	1.47	0.062	0.13
32	4.00	1.00	100.00	0.16	1.28	0.075	0.20

Table 3 Analysis of variance for main and interaction effects of parameters on R_a

Source	SS	*df*	MS	*F* value	Prob>*F*	For 95% level of confidence
Model	24.88	7	3.55	213.06	<0.0001	Significant
A	0.02	1	0.02	1.18	0.2885	
B	23.82	1	23.82	1,427.90	<0.0001	
C	0.59	1	0.59	35.44	<0.0001	
B2	4.69	1	4.69	281.06	<0.0001	
C2	0.17	1	0.17	10.47	0.0035	
AC	0.01	1	0.01	0.43	0.5194	
BC	0.07	1	0.07	4.42	0.0461	
Residual	0.40	24	0.02			
Lack of fit	0.27	19	0.01	0.53	0.8535	Not significant
Pure error	0.13	5	0.03			
Cor total	25.28	31				

gives the probability values associated with values that take the variable of a function of distribution *F*, for determined values of *df* of the numerator and the denominator.

3.2 Average surface roughness

Using ANOVA (Table 3), a second-order quadratic model was developed for R_a, as shown below in Eq. 1. The model was developed for 95% level of confidence. The model *F* value of 213.06 implies the model is significant. There is almost no influence, 0.01%, of noise on the model developed. By checking *F* value and *P* value, it is clearly seen that factor B (capacitance), factor C (voltage), and factor B^2 are most influential on R_a. The *P* value of each of these factors indicates the confidence level is more than 99.00%, which shows their very strong influence. The *P* value of interaction effects of BC shows the confidence level is above 95% and thus shows very good influence on R_a. The *P* value of factor A (feed rate) and interaction factor AC has insignificant influence over R_a as it provides very high *P* values. The lack of fit *F* value of 0.53 implies that the lack of fit is not significant compare to the pure error. The high *P* value of lack of fit, 85.35%, indicates the model is fit, while the very low *P* value of the model, 0.01%, indicates that the model is significant. The specific power transformation was chosen within the confidence level, which was suggested by the Design Expert software toolbox using Box-Cox plotting. In this case, natural log power transformation was suggested. Thus, the developed statistical quadratic equation for R_a is:

$$\begin{aligned} Ln(R_a) = &-7.956 - 0.044f + 1.423C + 0.087V \\ &- 0.111C^2 - 0.0004V^2 + 0.0006fV \\ &- 0.0007CV \end{aligned} \quad (1)$$

where,

f feed rate (μm s^{-1})
C capacitance (nF)
V gap voltage (V)

The effects of feed rate–voltage and capacitance–voltage on R_a are shown in Fig. 2, respectively. R_a is strongly influenced by capacitance and voltage. The increase of R_a

Table 4 Analysis of variance for main and interaction effects of the parameters on R_y

Source	SS	*df*	MS	*F* value	Prob>*F*	For 95% level of confidence
Model	20.04	7	2.86	88.23	<0.0001	Significant
A	0.12	1	0.12	3.85	0.0614	
B	18.68	1	18.68	575.88	<0.0001	
C	0.47	1	0.47	14.61	0.0008	
B^2	3.15	1	3.15	97.11	<0.0001	
C^2	0.10	1	0.10	3.19	0.0869	
AC	0.03	1	0.03	0.84	0.3687	
BC	0.28	1	0.28	8.77	0.0068	
Residual	0.78	24	0.03			
Lack of fit	0.69	19	0.04	2.02	0.2247	Not significant
Pure error	0.09	5	0.02			
Cor total	20.82	31				

Table 5 Analysis of variance for main and interaction effects of parameters on *TWR*

Source	SS	*df*	MS	*F* value	Prob>*F*	For 95% level of confidence
Model	0.1349	7	0.0193	196.57	<0.0001	Significant
A	0.0001	1	0.0001	0.91	0.3490	
B	0.0187	1	0.0187	191.14	<0.0001	
C	0.0090	1	0.0090	91.84	<0.0001	
A^2	0.0969	1	0.0969	988.02	<0.0001	
B^2	0.0025	1	0.0025	25.41	<0.0001	
AB	0.0001	1	0.0001	0.86	0.3637	
AC	0.0015	1	0.0015	15.58	0.0006	
Residual	0.0024	24	0.0001			
Lack of fit	0.0018	19	0.0001	0.94	0.5882	Not significant
Pure error	0.0005	5	0.0001			
Cor total	0.1373	31				

along with the increase in voltage is same as the conventional EDM. With the increase of capacitance from 0.1 to 5 nF, the R_a value increases but for further increase of capacitance the R_a values fall down. As the capacitance increased, large energy dissipated which erodes more materials with stronger spark. This strong spark erodes materials with high amount of debris from both the tool electrode and workpiece creating an uneven crater. As these debris are trapped in between the plasma channel, it causes unwanted spark. Thus, a high amount of discharge energy is employed to spark with debris, while work material is effectively removed by a small portion of discharge energy. Thus, lower R_a is obtained.

SEM surface textures of two machined surfaces with varying capacitance are shown in Fig. 3. In Fig. 3a, the surface texture was found very smooth (R_a=0.05 μm) with 0.1-nF capacitance while Fig. 3b shows comparatively rougher surface texture (R_a=0.22 μm) with the capacitance of 1 nF. The presence of unwashed debris was found responsible for higher roughness.

3.3 Maximum peak-to-valley roughness height

A second-order quadratic model was developed for R_y, as shown below in Eq. 2 using ANOVA (Table 4). This model was also developed for 95% level of confidence. The model *F* value of 88.23 implies the model is significant, with a negligible influence of noise. By checking *F* value and *P* value, it is clearly seen, like R_a, that factor B (capacitance), factor C (voltage), and factor B^2 are most influential on R_y. The *P* value of 99.00% of each of these factors indicates their very strong influence. The *P* value of interaction effects of BC shows the confidence level is above 95.0% and also shows very good influence on R_y. The high *P* value of factor A (feed rate) and interaction factor AC has insignificant influence. The lack of fit *F* value of 2.02 implies that the lack of fit is not significant compared to the pure error. The high *P* value of lack of fit, 22.47%, indicates the model is fit, while the very low *P* value of the model, 0.01%, indicates that the model is significant. Like R_a, natural log power transformation was

Table 6 Analysis of variance for main and interaction effects of parameters on *MRR*

Source	SS	*df*	MS	*F* value	Prob>*F*	For 95% level of confidence
Model	39.24	7	5.61	32.68	<0.0001	Significant
A	5.88	1	5.88	34.31	<0.0001	
B	7.90	1	7.90	46.03	<0.0001	
C	7.37	1	7.37	42.99	<0.0001	
A^2	9.33	1	9.33	54.37	<0.0001	
B^2	3.34	1	3.34	19.45	0.0002	
AB	2.21	1	2.21	12.88	0.0015	
AC	1.71	1	1.71	9.95	0.0043	
Residual	4.12	24	0.17			
Lack of fit	2.30	19	0.12	0.33	0.9636	Not significant
Pure error	1.82	5	0.36			
Cor total	43.36	31				

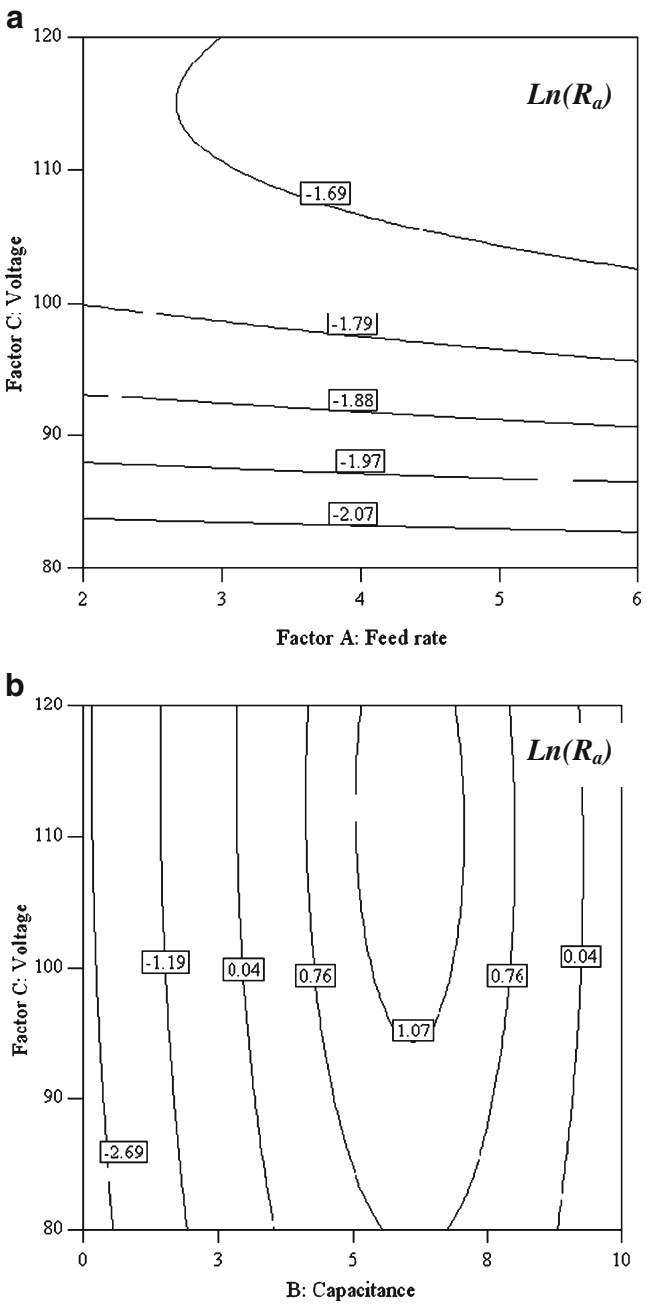

Fig. 2 Estimated response surface of R_a (μm): **a** $Ln(R_a)$ vs. f and V when C=1.0 nF, **b** $Ln(R_a)$ vs. C and V, when f=4.0 μm s^{-1}

also used for R_y. The developed statistical quadratic equation for R_y is:

$$Ln(R_y) = -4.981 - 0.077f + 1.264C + 0.07V - 0.091C^2 - 0.0003V^2 + 0.0012fV - 0.0014CV \quad (2)$$

The effects of feed rate–voltage and capacitance–voltage on R_y are shown in Fig. 4. The effects of capacitance and voltage on R_y are similar to the effects on R_a. But with the increase of feed rate at higher voltage, R_y increases steeper than R_a. The other effects are similar for both R_a and R_y.

3.4 Tool wear ratio

Using ANOVA, a second-order quadratic model was developed for *TWR* which is shown below in Eq. 3. Table 5 shows the model F value of 196.57, which implies the model is significant. There is less than 0.01% chance that this F value occurred due to noise. The F value and P value clearly shows that factor B (capacitance), factor C (voltage), factor A^2, factor B^2, and interaction factor AC are most influential on *TWR*. The P value of each of these factors indicates the confidence level is over 99%, which shows their very strong influence. The P value of factor A (feed rate) and interaction factor AB has insignificant effects over *TWR* as it provides very high P values. The lack of fit F value of 0.94 implies that the lack of fit is not significant compared to the pure error. The high P value of lack of fit, 58.82%, indicates the model is fit and the very low P value of the model, 0.01%, indicates that the model is significant. No power transformation was required for the modeling of *TWR*. Thus, the *TWR* statistical quadratic equation developed by the analysis is:

$$\mathrm{TWR} = 0.285 - 0.203f + 0.031C + 0.002V + 0.029f^2 - 0.003C^2 + 0.0002fC - 0.0003fV \quad (3)$$

The effects of feed rate–capacitance and feed rate–voltage on *TWR* are shown in Fig. 5. Capacitance and voltage strongly influenced the *TWR*, along with the interaction effect of feed rate–voltage. *TWR* decreases with the increase in feed rate. For further increase in feed rate, *TWR* starts rising. In the first phase, for a particular spark energy discharge, if the feed rate is so small, it will have high electron emission rate from the tool electrode, resulting in high *TWR*. As the feed rate increases, the spark energy is more involved in material erosion, which reduces *TWR* and reaches to minimum. In the second phase, for further increase of feed rate from the optimum, the unflashed eroded materials cause unwanted spark with the tool, which results in more tool wear. Thus, high *TWR* is obtained. With the increase in capacitance, large energy dissipated which produces stronger spark resulting in high work material erosion. Higher spark energy produces higher amount of debris. These debris sticking on the workpiece trap in and cause unwanted spark. The unwanted sparks erode materials from the tool electrode, which results in high tool wear. Thus, higher capacitance results in higher *TWR*. As

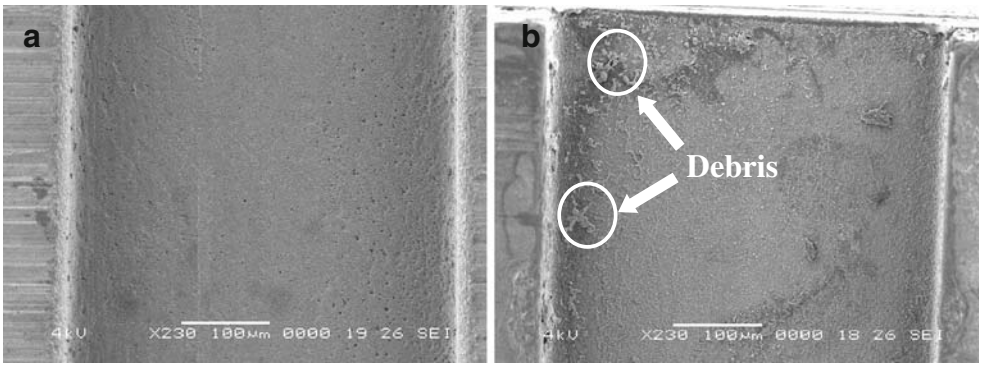

Fig. 3 SEM micrograph of the surface texture of micro ED-milled surface when feed rate= 4 μm s^{-1} and voltage=100 V, with varying capacitance of **a** 0.1 nF and **b** 1.0 nF

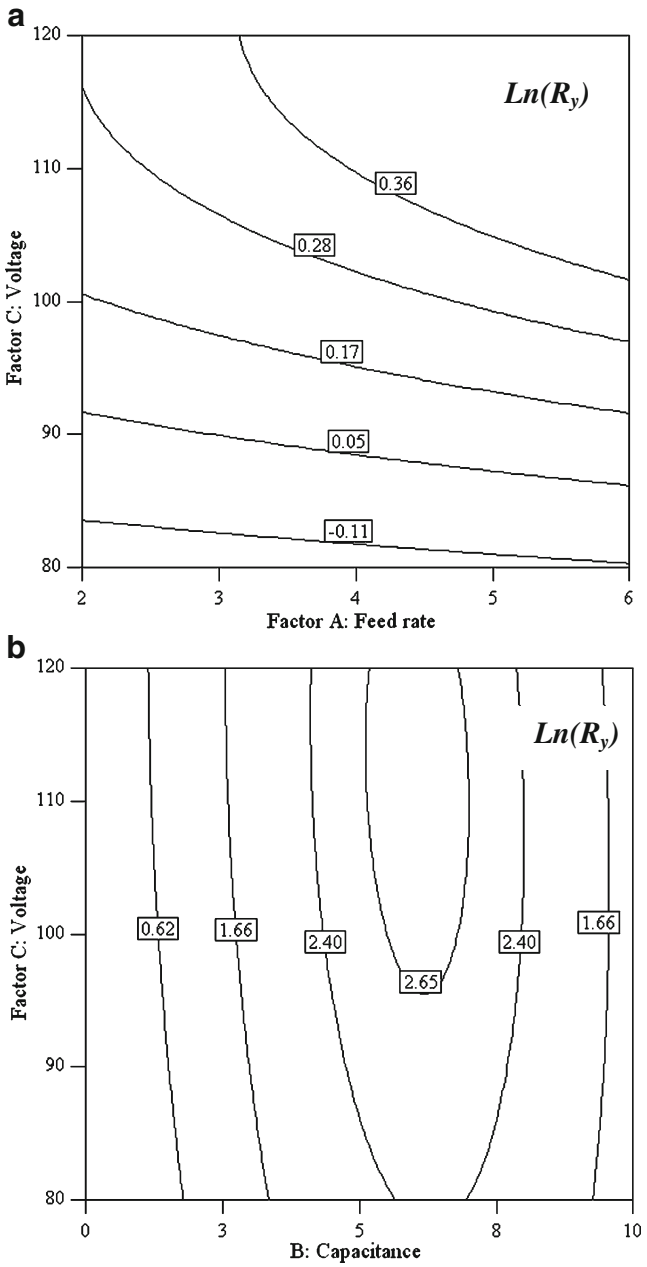

Fig. 4 Estimated response surface of R_y (μm): **a** $Ln(R_y)$ vs. f and V when C=1.0 nF, **b** $Ln(R_y)$ vs. C and V, when f=4.0 μm s^{-1}

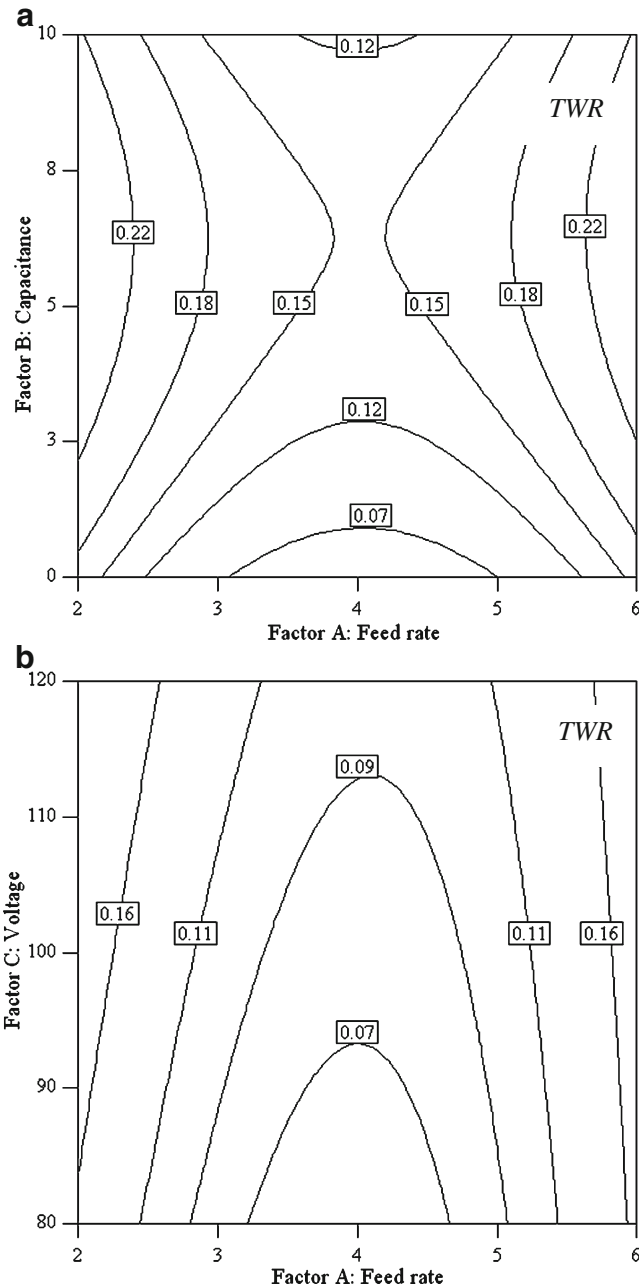

Fig. 5 Estimated response surface of *TWR*: **a** *TWR* vs. f and C when V=100 V, **b** *TWR* vs. f and V, when C=1.0 nF

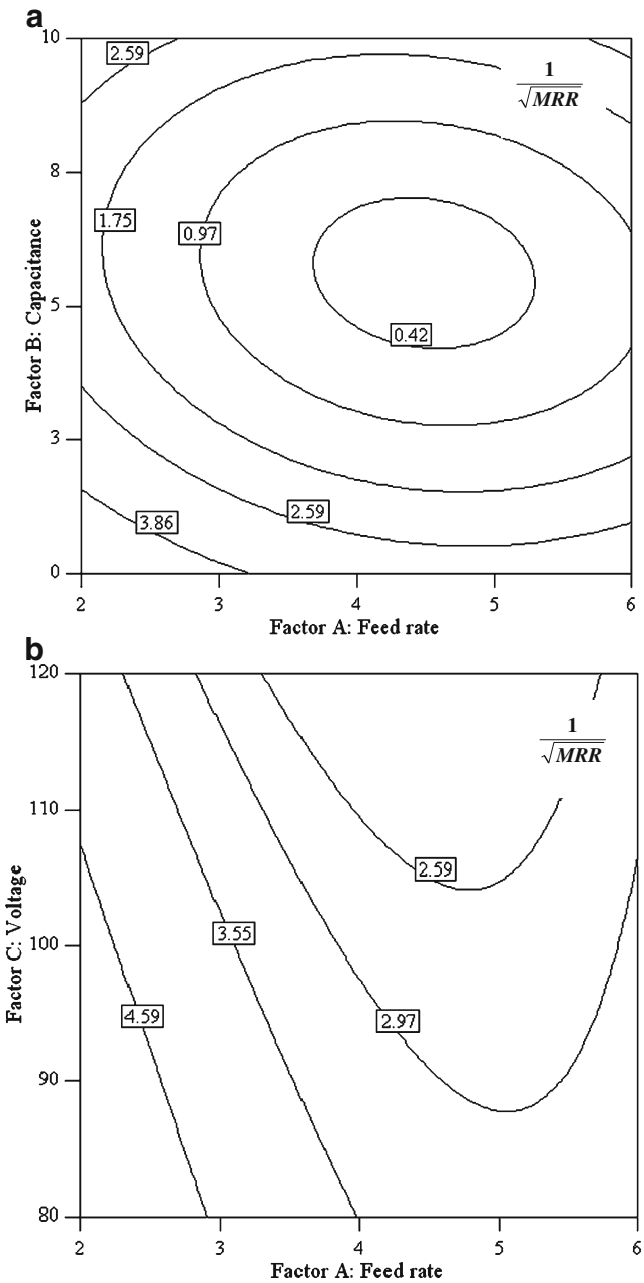

Fig. 6 Estimated response surface of *MRR* (mg min^{-1}): **a** $\frac{1}{\sqrt{\text{MRR}}}$ vs. f and C when V=100 V, **b** $\frac{1}{\sqrt{\text{MRR}}}$ vs. f and V, when C=1.0 nF

significant amounts of spark energy are employed in sparking with debris, the *MRR* decreases. *TWR* is a ratio of tool wear and workpiece wear, so decreases in *MRR* mean increase in *TWR*.

3.5 Material removal rate

The second-order quadratic model for *MRR* is developed, as shown in Eq. 4 by using ANOVA (Table 6). The model F value of 32.68 implies the model is significant because there is less than 0.01% chance that this model F value occurred due to noise. The F value and P values clearly shows that factor A (feed rate), factor B (capacitance), factor C (voltage), and factor A^2 are most influential on *MRR*. The P value of each of these factors indicates that the confidence level is over 99%, which shows their very strong influence. The P value of factor B^2, interaction factor AB, and interaction factor AC has also strong effects over *MRR* as it provides low P values. The lack of fit F value of 0.33 implies that the lack of fit is not significant compared to the pure error. The high P value of lack of fit, 96.36%, indicates that the model is fit while the very low P value of the model, 0.01%, indicates that the model is significant. The inverse square root power transformation was used for developing the model. The developed *MRR* statistical quadratic model is:

$$\frac{1}{\sqrt{\text{MRR}}} = 16.85 - 3.68f - 1.24C - 0.070V + 0.28f^2 + 0.09C^2 + 0.04fC + 0.01fV \quad (4)$$

The effects of feed rate and capacitance on $\frac{1}{\sqrt{\text{MRR}}}$ are shown in Fig. 6a, while the effects of feed rate and voltage are shown in Fig. 6b. *MRR* increases with the increase in feed rate. For further increase in feed rate, *MRR* starts falling slightly. As the feed rate increases, the spark energy is more involved in material erosion, which increases *MRR* till it reaches to the optimum. For further increase of feed rate from the optimum, the unflashed eroded materials cause unwanted spark with the tool, which changes the tool shape making it uneven and rough. The spark discharge results in reduced *MRR*. With the increase in capacitance, high energy dissipated which erodes more work materials with stronger spark. With the material erosion, the unflashed debris is trapped in between the machining zone and causes unwanted spark with the tool electrode. Thus, a portion of discharge energy is used to spark with debris. Hence, a lower amount of work material is eroded.

3.6 Multiple-response optimization

This subsection discusses the optimization of four output responses, R_a, R_y, *TWR*, and *MRR*. The developed nonlinear

Table 7 Values of process parameters for the optimization of R_a, R_y, *TWR*, and *MRR*

Feed rate (μm s^{-1})	Capacitance (nF)	Voltage (V)	R_a (μm)	R_y (μm)	*TWR*	*MRR* (mg min^{-1})	Desirability (%)
4.79	0.10	80.00	0.04	0.34	0.044	0.08	88.06

Table 8 Verification of multiple-response optimization

Desirability	Responses	Predicted	Actual	% Error
88.06%	R_a (μm)	0.04	0.04	0.00
	R_y (μm)	0.34	0.36	5.56
	TWR	0.044	0.053	16.98
	MRR (mg min^{-1})	0.08	0.09	11.11

models (Eqs. 1 to 4) are used for multiple-response optimization. In multiple-response case, it is complicated to find process parameters that simultaneously maximize or minimize all the responses as desired. Some tradeoffs are necessary in order to find process operating conditions that are satisfactory for most of the responses. There are several approaches to optimize multiple responses; among these, desirability function approach is most widely used. The method finds operating conditions, e.g., feed rate, capacitance, and voltage, that provide the "most desirable" values of the responses, e.g., R_a, R_y, *TWR*, and *MRR*.

In the analysis the objective function, $D(Yi)$, called the desirability function, reflects the desirable ranges for each response $Y_i(x)$ (where, $i=R_a$, R_y, *TWR*, *MRR*). For each response, a desirability function $d_i(Y_i)$ assigns numbers between 0 and 1 to the possible values of Y_i. $d_i(Y_i)=0$ represents a completely undesirable value of Y_i and $d_i(Y_i)=1$ represents a completely desirable or ideal response value.

The individual desirabilities are then combined using the geometric mean, which gives the overall desirability D:

$$D = \sqrt[n]{(d_1 \times d_2 \times ..... \times d_n)} = (d_1 \times d_2 \times ..... \times d_n)^{\frac{1}{n}} \quad (5)$$

where n is the number of responses in the measure. From the Eq. 5, it can be noticed that, if any response Y_i is completely undesirable ($d_i(Y_i)=0$), then the overall desirability is zero. In this case, the geometric mean of overall desirability is as follows:

$$D = \left(d_{R_a} \times d_{R_y} \times d_{TWR} \times d_{MRR}\right)^{\frac{1}{4}} \quad (6)$$

Depending on whether a particular response Y_i is to be maximized, minimized, or assigned a target value, different desirability functions $d_i(Y_i)$ can be used. In this case, R_a, R_y, and *TWR* are needed to be minimized while *MRR* needed to be maximized. Following are the two desirability functions:

$$d_i(Y_i) = \begin{matrix} 0 \\ \left(\frac{Y_i(x)-L_i}{T_i-L_i}\right)^s \\ 1.0 \end{matrix}, \quad \begin{cases} if & Y_i(x) \le L_i \\ if & L_i \le Y_i(x) \le T_i \\ if & Y_i(x) > T_i \end{cases} \quad (7)$$

$$d_i(Y_i) = \begin{matrix} 1.0 \\ \left(\frac{Y_i(x)-U_i}{T_i-U_i}\right)^s \\ 0 \end{matrix}, \quad \begin{cases} if & Y_i(x) \le T_i \\ if & T_i \le Y_i(x) \le U_i \\ if & Y_i(x) > U_i \end{cases} \quad (8)$$

where,

L_i Lower limit values
U_i Upper limit values
T_i Target values
s weight (define the shape of desirability functions)

Equations 7 and 8 are required when the goal is to maximize and minimize, respectively. The value of $s=1$ is chosen so that the desirability function increases linearly towards T_i.

The process parameters obtained by multiple-response optimization are shown in Table 7. For the shown values of process parameters, it is 88% desirable to get the R_a 0.04 μm, R_y 0.34 μm, *TWR* 0.044, and *MRR* 0.08 mg min^{-1}. Any other combination of the process parameters will either be statistically less reliable or give poor results of at least one of the responses. The analysis was done by using the Design Expert computer software.

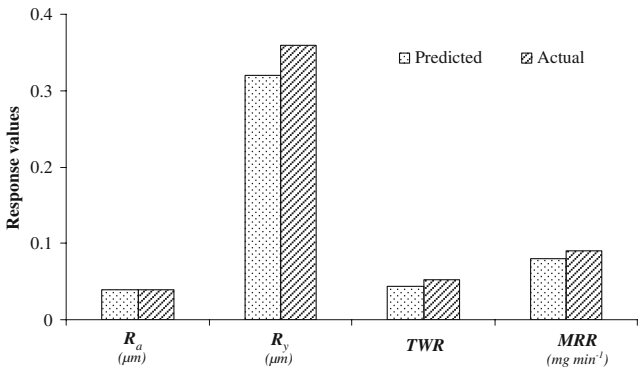

Fig. 7 Comparison of predicted vs. actual responses at a desirability of 88.06%

3.7 Verification of multiple-response optimization

Experiments were conducted to verify the result obtained from the multiple-response optimization (Table 7). The actual values obtained from the experiments are compared with the predicted values in Table 8. It can be noticed that

the predicted values of R_a show no error; R_y shows an error of 5.56%, while *TWR* shows the maximum error of 16.98% and *MRR* shows the error of 11.11%. *TWR* and *MRR* showed more percentage of errors compared to R_a and R_y. As *TWR* and *MRR* both are related to the material removal from the workpiece and/or tool, the low resolution (100 μg) of the electric balance is found as the possible contributor to this higher level of errors. This could be overcome either by prolonging the experiment time or by introducing a high resolution (e.g., 1 μg) electric balance. Figure 7 shows the comparison of predicted and actual values of the output responses.

4 Conclusions

This paper discusses the selection of micro ED milling parameters for the optimization of R_a, R_y, *TWR*, and *MRR*. Three-level full factorial experimental design was used for the statistical analysis. This study shows the followings:

1. R_a and R_y models (Eqs. 1 and 2) suggest that capacitance and voltage have strong individual influence on both the R_a and R_y, while the interaction effect of capacitance and voltage also affects those greatly. The effect of feed rate on R_y is found significant compared to R_a. Usually, higher discharge energy results in higher surface roughness. The unflashed debris sticking on the workpiece causes higher R_a and R_y. At very high discharge energy, the entrapped debris inside the plasma channel creates unwanted spark with the tool electrode. Thus, only a small portion of discharge energy involves in material erosion process, which results in low R_a and R_y.
2. *TWR* model (Eq. 3) shows that the capacitance and voltage have strong individual effects on *TWR* along with the interaction effect of feed rate and voltage. At high discharge energy, large amount of debris are produced, which causes high *TWR* by generating unwanted spark with the tool electrode.
3. *MRR* model (Eq. 4) shows that all the three parameters, feed rate, capacitance, and voltage, have strong individual and interaction effects on *MRR*. In general, high discharge energy results in high *MRR*. But the presence of high amount debris in the plasma channel often creates unwanted spark with the tool electrode. Thus, only a portion of energy involves in work material removal, which reduces *MRR*.
4. Multiple-response optimization shows 88.06% desirability for minimum achievable values of R_a, R_y, *TWR*, and maximum achievable *MRR*, which are 0.04, 0.34 μm, 0.044, 0.08 mg min^{-1}, respectively, when the feed rate, capacitance, and voltage are 4.79 μm s^{-1}, 0.10 nF, and 80.00 V, respectively. The obtained R_a and R_y values are in the acceptable range for many micro electromechanical applications.
5. Optimized machining parameters obtained from multiple-response optimization were used in verification experiments. The percentages of errors for R_a (0.0%) and R_y (5.56%) shows good prediction accuracy. Higher percentages of error were obtained for *TWR* (16.98%) and *MRR* (11.11%). Measurement inaccuracy due to low resolution (100 μg) of electric balance could be a reason behind this. By prolonging the experiment time or by introducing a high-resolution (1 μg) electric balance, this deficiency can be overcome.

References

1. Madou MJ (2002) Fundamentals of micro fabrication. The science of miniaturization, 2nd edn. CRC Press LLC, Boca Raton
2. Hsu TR (2002) MEMS & Microsystems- Design and Manufacture. McGraw Hill.
3. Ehmann KF, DeVor RE, Kapoor SG (2002) Micro/meso-scale mechanical manufacturing- opportunities and challenges. Proc JSME/ASME Int Conf Mater Process 1:6–13
4. Lim HS, Wong YS, Rahman M, Lee MKE (2003) A study on the machining of high-aspect ratio micro-structures using micro-EDM. J Mater Process Technol 140:318–325 doi:10.1016/S0924-0136(03)00760-X
5. Fleischer J, Kotschenreuther J (2007) The manufacturing of micro molds by conventional and energy-assisted processes. Int J Adv Manuf Technol 33:75–85 doi:10.1007/s00170-006-0596-1
6. Puertas I, Luis CJ (2004) A study of optimization of machining parameters for electrical discharge machining of boron carbide. Mater Manuf Process 19(6):1041–1070
7. Lin YC, Cheng CH, Su BL, Hwang LR (2006) Machining characteristics and optimization of machining parameters of SKH 57 high-speed steel using electrical-discharge machining based on Taguchi method. Mater Manuf Process 21(8):922–929
8. Uhlmann E, Piltz S, Jerzembeck S (2005) Micro-machining of cylindrical parts by electrical discharge grinding. J Mater Process Technol 160:15–23 doi:10.1016/j.jmatprotec.2004.02.054
9. Han F, Jiang J, Yu D (2007) Influence of machining parameters on surface roughness in finish cut of WEDM. Int J Adv Manuf Technol 34(5–6):538–546
10. Chiang K (2007) Modeling and analysis of the effects of machining parameters on the performance characteristics in the EDM process of Al2O3+TiC mixed ceramic. Int J Adv Manuf Technol 37(5–6):528–533
11. Liao YS, Huang JT, Chen YH (2004) A study to achieve a fine surface finish in wire-EDM. J Mater Process Technol 149:165–171 doi:10.1016/j.jmatprotec.2003.10.034
12. Salonitis K, Stournaras A, Stavropoulos P, Chryssolouris G (2007) Thermal modeling of the material removal rate and surface roughness for die-sinking EDM. Int J Adv Manuf Technol ISSN 0268-3768 (Print) 1433-3015 (Online)doi:10.1007/s00170-007-1327-y
13. Her M-G, Weng F-T (2001) Micro-hole machining of copper using the electro-discharge machining process with a tungsten carbide electrode compared with a copper electrode. Int J Adv Manuf Technol 17:715–719 doi:10.1007/s001700170116
14. Kim YT, Park SJ, Lee SJ (2005) Micro/meso-scale shapes machining by micro EDM process. Int J Prec Engin Manuf 6(2):5–7

15. Ozgedik A, Cogun C (2006) An experimental investigation of tool wear in electric discharge machining. Int J Adv Manuf Technol 27:488–500 doi:10.1007/s00170-004-2220-6
16. Son SM, Lim HS, Kumar AS, Rahman M (2007) Influences of pulsed power condition on the machining properties in micro EDM. J Mater Process Technol 190:73–76 doi:10.1016/j.jmatprotec.2007.03.108
17. Lee SH, Li XP (2001) Study of the effect of machining parameters on the machining characteristics in electrical discharge machining of tungsten carbide. J Mater Process Technol 115:344–358 doi:10.1016/S0924-0136(01)00992-X
18. Chen SL, Yan BH, Huang FY (1999) Influence of kerosene and distilled water as dielectrics on the electric discharge machining characteristics of Ti-6Al-4V. J Mater Process Technol 87:107–111 doi:10.1016/S0924-0136(98)00340-9
19. Chung KD, Kim BH, Chu CN (2007) Micro electrical discharge milling using deionized water as a dielectric fluid. J Micromech Microeng 17:867–874 doi:10.1088/0960-1317/17/5/004
20. Ghoreishi M, Atkinson J (2002) A comparative experimental study of machining characteristics in vibratory, rotary and vibro-rotary electrodischarge machining. J Mater Process Technol 120:374–384 doi:10.1016/S0924-0136(01)01160-8